University of Copenhagen
Niels Bohr Institute
Center for Quantum Devices

Bachelor Thesis

Dispersive Readout in Mesoscopic Structures

Author:
Thorvald Wadum Larsen

Supervisor:
Charles M. Marcus

12. April 1991

June 12, 2013

Abstract

Semiconductor based quantum information processing is a promising platform for realizing the quantum computer. Fast readout of individual qubits is an essential ingredient in most quantum information proposals. Fast readout has been demonstrated in semiconductor quantum dot qubits, but it requires the use of an additonal sensor dot. This added complexity becomes a considerable burden as the number of qubits is scaled.

Dispersive readout is a recently developed alternative technique that avoids the use of a sensor dot. However, in its current form, its sensitivity does not meet the stringent requirements needed for a quantum computer.

Using numerical simulations and a model circuit at cryogenic temperatures, I show that a simple alteration to the currently used circuit could make dispersive readout 22 times faster. This improvement promises dispersive readout as a viable option for quantum computation with spin qubits because it will allow for single-shot readout of the qubit state. My results are applicable to a wide range of quantum dot qubits in systems such as 2D semiconductor heterostructures, carbon nanotubes, and semiconductor nanowires.

Acknowledgements

I thank Charles M. Marcus, Ferdinand Kuemmeth, and Andrew Higginbotham for invaluable discussions and input for the work at hand. In Addition I would like to give a special thanks to A. Higginbotham for teaching me the ins and outs of quantum electronic experiments in a dilution refrigerator.

Contents

List of Figures

1 Introduction

Quantum information processing promises novel possibilities in programming and data manipulation [1]. Quantum computations are done on qubits, a bit that is in a superposition of 1 and 0. Processing on qubits can be viewed as coherent parallel classical processes done on boolean bits. In [2] the experimental requirements to build a quantum computer is specified: Scalable qubit system, Initialization, one- and two-qubit operations and readout of individual qubits. Mesoscopic structures in semiconductors has proven to be a plausible path to meet these criteria.

The spin degree of freedom of a quantum dot can be used to store quantum information [3]. In GaAs, such a spin qubit has been realized [4]. A high level of coherence [5], and strong qubit-qubit coupling [6] have been demonstrated in this architecture. Of particular importance to this work, single-shot readout of the qubit spin has also been demonstrated [7].

The readout technique used in [7] uses a capacitively coupled sensor quantum dot to determine the spin state of the qubit. While this technique is extremely sensitive ($\sim$10 microsecond readout time), the complexity introduced by an additional sensor dot is burdensome.

To solve this problem recently dispersive readout of the quantum state has been demonstrated, which neglects the need for a separate mesoscopic detector making scaled-up arrays of qubits imaginable [8].

The focus of this thesis is to improve the sensitivity of the dispersive readout technique. This is achieved by making a simple adjustment to the current readout circuit. The new readout readout scheme is then modelled to an effective circuit, which was simulated to investigate its behaviour. To back up the simulations the circuit was build and analysed to prove or disprove the validity of the simulated model. Experiments was done in a dilution refrigerator with a base temperature below 50mK to replicate experimental environment.

The thesis is organized as follows. First I introduce a capacitive model of single and double quantum dots (DQD) and describe the singlet-triplet qubit in a DQD including a presentation of charge sensing and dispersive readout (sec. 2). The next section is devoted to the readout technique reflectometry, which is an essential part of fast charge sensing and dispersive readout (sec. 3). I then show the results from simulations on the behaviour of the adjusted readout scheme for dispersive readout including simulated measurements (sec. 4). Lastly the experimental results of the proposed readout scheme is presented and compared to the simulation (sec. 5).

2 Mesoscopic structures

2.1 Capacitive model of quantum dots

Quantum dots in mesoscopic structures can be described by the classical capacitive model [9]. The model is presented in an electron system, but everything also applies for a hole system if the appropriate signs are changed.

The quantum dot In the capacitive model we assume the dot to be an island connected to contacts via tunnel resistors and capacitors and capacitively coupled to a gate, figure 1. The number of electrons in the dot is denoted N. $R_{R(L)}$ and $C_{R(L)}$ are the tunnel resistor and capacitor from the right (left) contact to the dot. The gate voltage V_g is coupled to the dot through the capacitor C_g. In the capacitive model we can calculate the charge on the dot, Q, as the sum of charges on each capacitor to the dot.

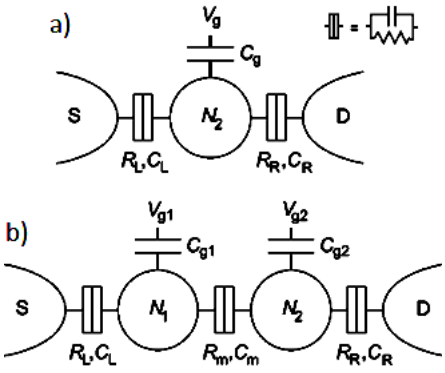

Figure 1: Capacitive model of a) a quantum dot and b) a double quantum dot. All stray and cross capacitances are assumed to be negligible. Figure adopted from [9].

$$\begin{aligned} Q =& C_L(V_1 - V_L) + C_g(V_1 - V_g) + C_R(V_1 - V_R) \quad \Leftrightarrow & (1)\\ \varepsilon C_1 V_1 =& Q + C_L V_L + C_g V_g + C_R V_R & (2) \end{aligned}$$

Where $V_{L(R)}$ is the potential on the left (right) lead, V_1 is the dot potential, and $C_1 = C_L + C_g + C_R$ is the total capacitance on the dot. The electrostatic energy, U, can now be calculated as the capacitive energy on the dot,

$$U_N = \frac{1}{2} C_1 V_1^2 = \frac{(C_1 V_1)^2}{2C1} = \frac{(-(N - N_0)e + C_L V_L + C_g V_g + C_R V_R)^2}{2C_1} \tag{3}$$

Where we have substituted the charge, Q, with $-(N_1 - N_0)e$, where e is the electron charge and N_0 the number of electrons on the dot when all voltage sources are zero. The N_0 electrons compensate for the positive background of the donors in the semiconductor. With an expression for the electrostatic energy we can calculate the electrostatic potential, μ, of the dot,

$$\begin{aligned} \mu(N) &= U_N - U_{N-1} \\ &= \frac{[-(N - N_0)e + C_L V_L + C_g V_g + C_R V_R]^2}{2C_1} \\ &\qquad - \frac{[-((N-1) - N_0)e + C_L V_L + C_g V_g + C_R V_R]^2}{2C_1} \\ &= \frac{(N - N_0)^2 e^2 - ((N-1) - N_0)^2 e^2}{2C_1} - \frac{2(N - N_0)e\,(C_L V_L + C_g V_g + C_R V_R)}{2C_1} \\ &\qquad + \frac{2((N-1) - N_0)e\,(C_L V_L + C_g V_g + C_R V_R)}{2C_1} \\ &= \frac{(2(N - N_0) - 1)e^2 - 2e\,(C_L V_L + C_g V_g + C_R V_R)}{2C_1} \end{aligned} \tag{4}$$

This is a purely classical model. Quantum mechanics adds an extra term to the electrostatic energy (3) in the form of single-particle energies, $\sum_{n=1}^{N} E_n$. The energy E_n is the single-particle energy of the n'th electron which depends on the confinement potential. In the electrostatic potential this introduces the level spacing $\Delta E_N = \sum_{n=1}^{N} E_n - \sum_{n=1}^{N-1} E_n = E_N - E_{N-1}$ and becomes the electrochemical potential,

$$\mu(N) = \frac{e^2}{C_1}\left(N - N_0 - \frac{1}{2}\right) - \frac{e}{C_1}\left(C_L V_L + C_g V_g + C_R V_R\right) + \Delta E_N \tag{5}$$

We can see that the electrostatic potential, or the energy level, of the dot depends linearly on the gate voltage, figure 2a. The sawtooth shape appears due to electrons jumping into the dot. This happens, in the case of zero bias across the dot, only when the electrostatic potential of the dot is equal to the leads. Electrons on the dot with an energy below the electrochemical potential of the leads cannot jump off, because there is no available energy states on the leads.

Electrons can only jump onto or off the dot when the energy level of the dot aligns with that of the leads. Anywhere else the electrons on the dot are trapped and block new electrons from entering. This implies that there cannot run a current through the dot away from alignment, a phenomenon called coulomb blockade, figure 2b. When the levels align electrons can jump onto and off the dot freely and thereby allow a current flow through the dot, figure 2c. These peaks in the current as a function of gate voltage are called coulomb peaks, figure 2d.

Quantum dots have been realized in many forms f.ex. the single electron resistor (SET) [10], semiconductor heterostructure, semiconductor nanowires and superconductors.

The double quantum dot Putting two quantum dots in series we get a DQD, figure 1b, where $N_{1(2)}$ is the number of electrons on the left (right) dot and C_m is the mutual capacitance between the dots. The calculations for such a dot is the same as before although they get quite long. Therefore I will just present the result obtained, under the assumption that the stray and cross capacitances are negligible, in [9]. These results are for the zero bias regime where $V_R = V_L = 0$.

$$\mu_1(N_1, N_2) = \left(N_1 - \frac{1}{2}\right) E_1 + N_2 E_2 - \frac{1}{e}\left(C_{g1} V_{g1} E_1 + C_{g2} V_{g2} E_m\right), \tag{6}$$

$$\mu_2(N_1, N_2) = \left(N_2 - \frac{1}{2}\right) E_2 + N_1 E_1 - \frac{1}{e}\left(C_{g1} V_{g1} E_m + C_{g2} V_{g2} E_2\right). \tag{7}$$

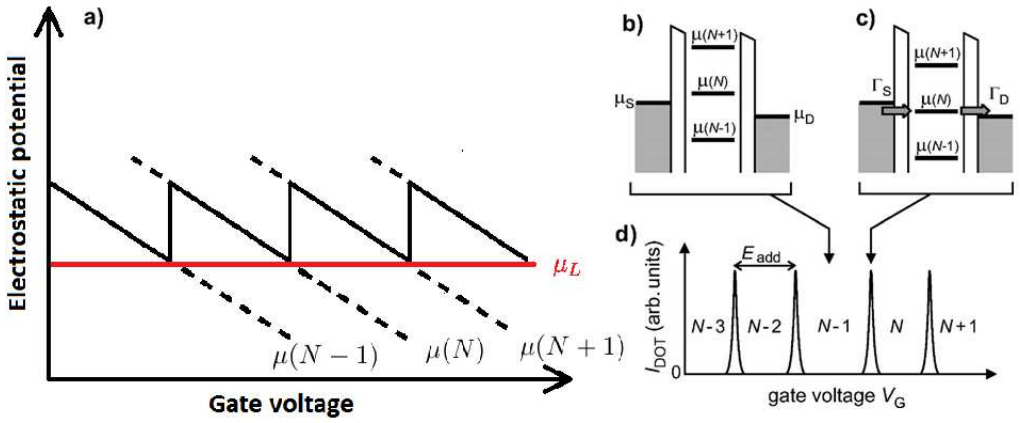

Figure 2: a) The electrostatic potential μ of a quantum dot as a function of gate voltage. b) The energy levels in a quantum dot in the coulomb blockade regime. c) Energy levels at a coulomb peak. d) Current as a function of gate voltage with bias approximately zero showing coulomb peaks. Figure b-d from [11].

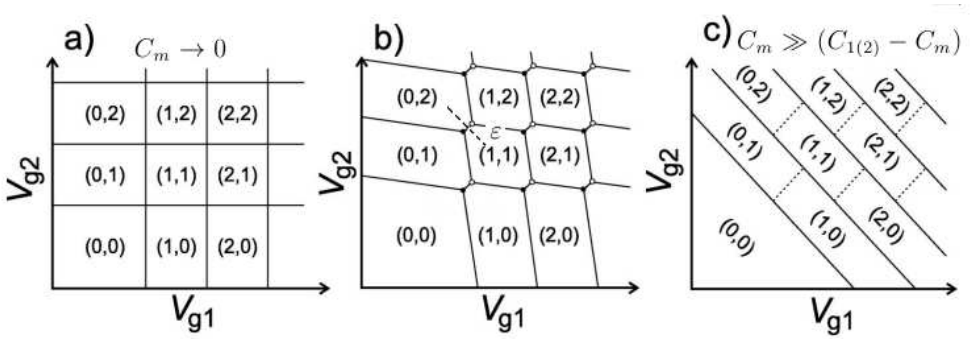

Figure 3: Stability diagram for a DQD for different regimes of coupling capacitance C_m.The stable charge configuration of the dot is denoted (N_1, N_2). a) No coupling regime. b) Weak coupling regime. The dashed line is defined as detuning ε. c) Strong coupling regime. Figure from [9].

Where $E_{1(2)} = \frac{e^2}{C_{1(2)}} \left(\frac{1}{1 - \frac{C_m^2}{C_1 C_2}} \right)$, $E_m = \frac{e^2}{C_m} \left(\frac{1}{\frac{C_1 C_2}{C_m^2} - 1} \right)$ and $C_{1(2)} = C_{L(R)} + C_{g1(2)} + C_m$ is the sum of capacitances on dot 1(2). With these equations it is possible to draw a stability diagram figure 3. In a stability diagram crossing a line means that the otherwise stable system changes. In this case there is either an electron jumping onto a dot or off a dot. This electron can go to or come from either the lead or the other dot. The stable charge configuration of the dot is denoted (N_1, N_2).

Letting C_m go to zero we obtain the stability diagram shown in figure 3a. This is two completely decoupled dots in series. Going to the other limit $C_m \gg (C_{1(2)} - C_m)$ we have one dot with two gates connected to it, figure 3c. In between these limits we find the weakly coupled DQD, figure 3b.

A electron microscope picture of a semiconductor DQD is shown in figure 4c. The gates are denoted by L and R. The gate G controls the interdot tunnel coupling C_m.

2.2 Spin-qubits in semiconductors

To make quantum operations we need to be able to store the quantum information. Almost any interaction with the parameter that stores the quantum information will destroy it. The spin couples only weakly to the environment making it an attractive place to store quantum information. This is called a spin-qubit, a qubit where the information is stored in the spin state of the system.

Spin manipulation in a quantum dot It is possible to trap a single electron in a quantum dot. The ground state of the single electron is double degenerate in zero magnetic field. The electron has either spin up or spin down. When a magnetic field is applied the degeneracy of the dot is lifted due to the Zeeman effect. The spin of the electron couple to the magnetic field which splits the energy level of the spin up and spin down states. The size of the splitting is called the Zeeman energy.

With the two levels split with a finite magnetic field it is possible to distinguish the two electron states, by exploiting the fact that the two spin states have different energy levels. If the levels are slowly raised by applying a voltage on the gate, the spin state with the highest energy will be able to jump out of the dot before the lower lying spin state. Allowing for distinguishing the two spin states via the charge on the dot. This is called spin to charge conversion.

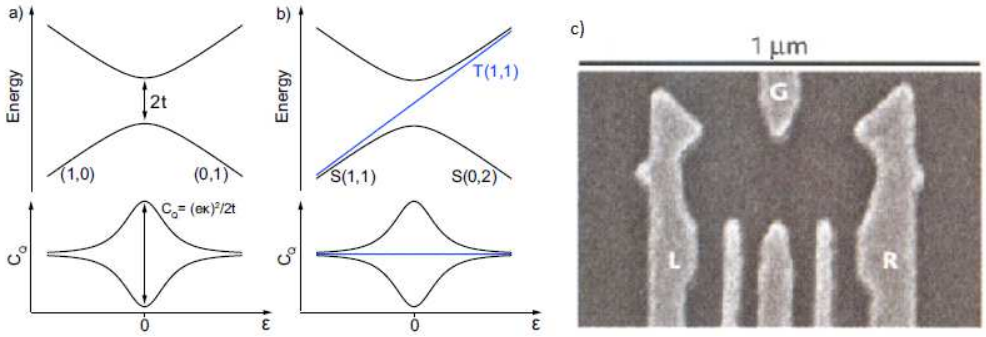

Figure 4: a) Energy diagram of a single electron in a DQD. Below the quantum capacitance of the electron. b) Two electron in a DQD showing the anticrossing of the single state. c) Electron microscope picture of a semiconductor DQD. Figures a) and b) from [13], figure c) from [4].

The singlet-triplet spin-qubit In a DQD it is possible to realize a qubit by looking at the singlet and triplet spin states. The combined spin of two electrons in a DQD can be in the antisymmetric singlet state or one of the three symmetric triplet states. Applying a magnetic field through the DQD will split the otherwise degenerate triplet spin states. We define detuning, ε, as $\varepsilon = \frac{V_{g2} - Vg1}{2}$ along the dotted in figure 3b. Right between the $(1,1)$ and $(0,2)$ regimes detuning is zero. Positive detuning is in the $(0,2)$ charge configuration and negative detuning in $(1,1)$. The detuning is a measure of how much the potential across the two dots are tilted.

The energy diagram shows in the top part of a) the hybridization of the $(1,0)$ state and $(0,1)$ for a single electron in a DQD. Top b) shows the hybridization of the $S(1,1)$, where $S(1,1)$ indicates it is a singlet $(1,1)$ state, and the $S(0,2)$ states in zero magnetic field. The hybridization creates an anti-crossing. There is similar anti-crossings for the three triplet states at higher detuning.

The amount of energy it takes to move the electrons into the $(0,2)$ configuration depends on whether the electrons is in a spin-singlet, S, or spin-triplet state, T. If the electrons are in the antisymmetric spin-singlet state they can both occupy the lowest lying orbital in one dot. This is not possible for the symmetric spin-triplet state due to Pauli's exclusion principle. Pauli's exclusion principle states that fermions cannot have all the same quantum numbers. From this it can be worked out that the many-body wave function of fermions has to be antisymmetric.

The spin-triplet state is symmetric leading to the orbital state of the two electrons being antisymmetric. This is only possible by including a higher lying orbital in the orbital wave function when they occupy the same dot, which is why the hybridization between the $T(1,1)$ to $T(0,2)$ lies at much higher detuning and energy than that of the $S(1,1)$ and $S(0,2)$.

This mechanism can be observed in a phenomenon called spin-blockade. Preparing a state in the $(1,1)$ configuration we have either a spin singlet or a spin triplet state. Then moving to a positive detuning that is high enough than the $S(1,1)$ goes into the $S(0,2)$, but lower than the crossover between the $T(1,1)$ to $T(0,2)$. The spin singlet will immediately go into the $(0,2)$ configuration while the triplet state will stay in $(1,1)$. In this way it is possible to distinguish the singlet and triplet state via the charge distribution allowing for spin to charge conversion in the singlet-triplet spin-qubit.

When a measurement of the qubit state is done via spin-blockade, the triplet and singlet state are energetically split, introducing a relaxation from the higher lying triplet state to the lower singlet state with the characteristic time scale T_1. Any quantum

operation or readout has to be done faster than T_1. If the measurement takes longer there will be chance that the triplet state relaxes into the singlet state in the middle of the operation giving a wrong result.

2.3 Transport

Measuring the state of a quantum dot or DQD can be done in many ways. The easiest is to measure the conductance of the system. That is the transport through the system. For a quantum dot it is possible to map out the energy spacing in the dot both with the gate voltage and bias across the dot. This allows for a measurement of the electron temperature. When applying a magnetic field, and thereby splitting the energy levels it is possible to measure the magnetic g-factor of the system via transport.

In the case of a DQD transport allows us to map out stability diagrams of the system, here is briefly presented the case of zero bias. There will be a current running at the points where the chemical potential of both dots align with that of the leads. This happens when three lines meet in the stability diagram. Along the lines in the stability diagram, where the energy level in one dot aligns with the leads, there will be a small amount of current, depending on the hight of the barriers. From the stability diagram the amount of electrons in the dot can be deduced. This is done simply by finding the lowest transition and assume that there is zero electrons in the dot below.

Transport in mesoscopics is a whole topic in itself and is described in more detail in f.ex. [9] and [11].

2.4 Charge sensing

When doing transport measurements you run a current of millions of electrons through a dot. If we want to do quantum processing with a spin-qubit we want to measure the spin state of a single electron. This is not possible with transport measurements. Instead we want to measure the charge distribution in the system while disturbing the system as little as possible.

Mapping out an image of the charge distribution is not possible. But it is possible to measure changes in the charge distribution due to f.ex. one electron jumping off a dot. This is done with a mesoscopic charge sensor [12], which can be a qauntum dot or a quantum point contact (QPC). The principle is the same in both cases. Looking at the conductance as a function of gate voltage we see steps in a QPC and coulombs peaks in the quantum dot. First we want to navigate the gate voltage such that we are on a sharp side of a step or a peak respectively. This means that the conductance is very sensitive to changes in electrical potential around it. If the mesoscopic sensor is placed close to a dot, the dot will work as a gate on the sensor. When an electron jumps off the dot it will gate the sensor a little less, and thereby changing the conductance through the sensor.

In the case of a singlet-triplet qubit we want to detect whether both electrons moves into the $(0, 2)$ charge configuration at positive detuning implying a singlet state or stay in the $(1, 1)$ implying a triplet state. This can be seen as different charge distributions which is detectable with a nearby mesoscopic charge sensor.

2.5 Dispersive response

Electrons couple capacitively to the surroundings, a phenomenon called quantum capacitance. The quantum capacitance of an electron is suppressed when undergoing tunnelling. When the energy level of a dot aligns with that of a lead there will be electrons tunnelling onto and off the dot even if there is no current through the dot. This can happen if one side of a quantum dot is pinched off. Also in a DQD when the two

energy levels of the dots aligns there will be tunnelling between the two dots suppressing quantum capacitance.

The quantum capacitance of a DQD can be calculated as a function of detuning [13]. The quantum capacitance is proportional to the curvature of the energy level,

$$C_Q = -(e\kappa)^2 \frac{\partial^2 E}{\partial \varepsilon^2}. \tag{8}$$

where κ is a coupling factor between the measurement voltage V and detuning, $\Delta\varepsilon = -e\kappa\Delta V$, and E the energy level. For a single electron in a DQD we find that there is a change in the quantum capacitance as it moves from one dot to the other , bottom part of figure 4a . The picture is the same for the singlet $S(1,1)$ in the two electron case, while the triplet state response will be seen at a higher detuning where the hybridization is located , figure 4b.

3 Reflectometry

Operations done on qubits needs to be done faster than the relaxation time, T_1, of the system. Measurements done with charge sensing is limited by the RC time of the charge sensor, the resistance through the conductance and the capacitance to room temperature where we measure the system. These numbers are typically $R > 50\text{k}\Omega$ and C hundreds of picofarads limiting bandwidth of the charge sensor to less than 100kHz. Ideally measurements should be performed on the timescale of qubit relaxation/decoherence. In the case of GaAs singlet-triplet qubits, this requires measurements bandwidths of roughly 1 MHz. To allow operations on quantum information we need a much higher bandwidth. This can be accomplished by the implementation of reflectometry.

Reflectometry was first implemented in a SET based charge sensor [14]. Using the same principle the RF-QPC was demonstrated [15] and [16]. Later reflectometry was used to make dispersive readout [13]. The principle of reflectometry is to measure the reflected signal from a resonant circuit. The quality of the resonance depends on the specific electrical components. Changes in the resonance is connected to a change in the components, making it possible to detect these changes in the reflected signal.

I will first present the tank circuit which is the circuit connecting the room temperature instruments to the device and allows manipulation and readout of the high frequency signal used in reflectometry. Following after is a description of the readout circuits used in reflectometry.

3.1 Tank circuit

The tank circuit is the circuit going down to the readout circuit and up again. A possible configuration, and the one I used, is shown in figure 5. In the actual circuit there is also high and low pass filters to minimize noise.

Starting from the signal generator. We first split the signal into a carrier line (blue arrow on figure) and a reference line (yellow arrow). Following the carrier we hit a switch, which allows us to turn on and off the carrier signal on a much shorter time scale than is possible with the signal generator. This minimizes the back action onto the sample. The phase shifter is in place to allow tuning of the readout phase. Before we reach the sample we need to attenuate the signal to avoid blowing up the sample. This also helps with thermalization of the signal. The directional coupler sends the carrier signal down one line and the reflected signal (green arrow) up another line.

The reflected signal is the part of the carrier that is reflected from the sample and the readout circuit. Only a negligible amount of the reflected signal is transmitted through the directional coupler back up the carrier line. After the coupler the signal is amplified

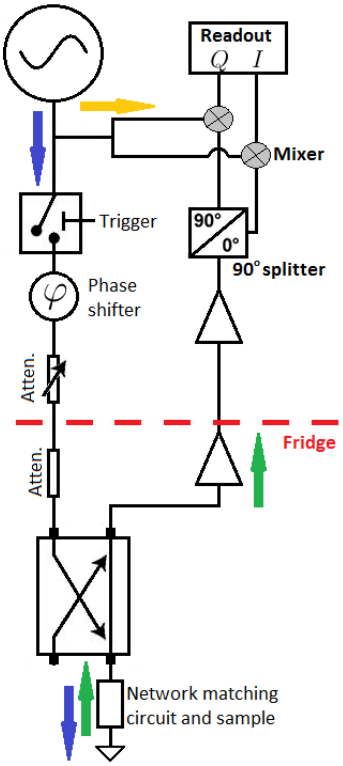

Figure 5: Tank circuit used to do reflectometry measurements. Blue arrow: Carrier signal. Green arrow: Reflected signal. Yellow arrow: Reference signal.

with a cryogenic amplifier, which has a high gain of 47dB and a low noise temperature of 4K in optimal settings, and other room temperature amplifiers. The important part is that the first amplifier has a very low noise level, because the noise from this amplifier is amplified by the following amplifiers.

The amplified signal is measured using what is basically a high bandwidth lock-in amplifier (although there is no further amplification). We split the signal with a 90°-splitter to allow readout of both the real part, I, and the imaginary part, Q. With the phase shifter on the carrier line it is possible to tune the split such that we get I and Q. Following the splitter the two parts of the reflected signal is mixed with the reference signal giving us an easy measurable DC signal. Contrary to what it looks like on the figure the two reference lines have the same length such that we really get a 90° split readout.

3.2 Readout circuit

We now turn our attention to the readout circuit and sample, that creates the resonance we are measuring. The basic idea behind the readout circuit is to create a resonance that reacts to changes is the electrical component we want to measure. The reflected can be calculated from the effective impedance of the readout circuit, Z_{eff}, and the impedance of the source, Z_0. Here the impedance of the source is the 50Ω characteristic impedance of the coax line. The reflection coefficient, S_{11}, is given by:

$$S_{11} = \frac{Z_0 - Z_{\text{eff}}}{Z_0 + Z_{\text{eff}}} \tag{9}$$

This coefficient is the ratio of the voltage that is reflected. The power reflection coefficient, the ratio of power that is reflected, is the square of the reflection coefficient S_{11}. This can be seen by,

$$\frac{P_{\text{Refl}}}{P_0} = \frac{(V_{\text{Refl,rms}})^2}{(V_{0,\text{rms}})^2} = \frac{(V_{\text{Refl}})^2}{(V_0)^2} = (S_{11})^2 \tag{10}$$

Where P_{Refl} is the power reflected and P_0 the incident power.

Resistive reflectometry We want to measure a purely resistive signal in a mesoscopic charge sensor. In reflectometry this is translated into a resonance by a network matching circuit, consisting of an inductor L and the parasitic capacitance C_p in the sample. The matching circuit is presented in figure 6a, R_l is the line resistance and R is the resistance of the sensor. From there it is easy to find the effective impedance off the circuit:

$$Z_{\text{eff}} = i\omega L + R_l + \frac{1}{i\omega C_p + \frac{1}{R}} \tag{11}$$

From equation (9) we can see that when Z_{eff} is equal to Z_0 there is no reflection. This condition is met when[1]

$$Z_0 = \frac{L}{RC_p} - R_l \qquad \text{and} \qquad f_0 = \frac{1}{2\pi\sqrt{LC_p}} \tag{12}$$

The amount of reflected signal depends on R. This allows detection changes in R just by monitoring the reflected signal. With this method it is possible to measure conductance changes at a much faster rate than transport measurements.

In 2005 this method was used to demonstrate real time current measurements [17]. This was done with a SET close to the current flow. The change in charge distribution due to one electron passing by was then measured and counted. The mesoscopic charge sensor can also be a QPC or a quantum dot. In 2010 it was investigated which charge

[1] To get this result the I have made the approximation $\frac{1}{L} \gg \frac{1}{C_p R^2}$

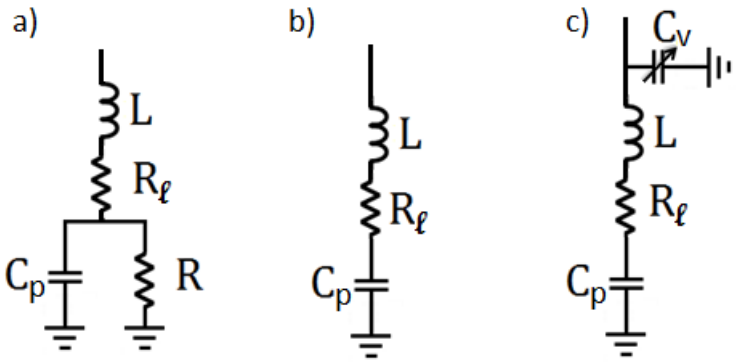

Figure 6: Three circuits used for reflectometry where the inductor is denoted L, the parasitic capacitance C_p, the line resistance R_l. a) Circuit used for measuring R, f.ex. an RF-QPC. b) Circuit to measure the parasitic capacitance, C_p. c) Proposed improvement to the circuit in b).

detector gives the best reflectomtry readout [18]. It was found that the RF-quantum dot is 30 times more sensitive than the RF-QPC.

Capacitive readout As introduced in section 2.5 the quantum capacitance of an electron changes in experiments. This was exploited in semiconductor qubit systems, where dispersive readout with reflectometry on the lead of a DQD was demonstrated [13]. The change in quantum capacitance shows up in the parasitic capacitance. The model for dispersive readout is presented in 6b. This is basically a RLC-circuit with an effective impedance given by,

$$Z_{\text{eff}} = i\omega L + R_l + \frac{1}{i\omega C_p} \tag{13}$$

The resonance frequency is the same as before, $f_0 = \frac{1}{2\pi\sqrt{LC_p}}$, while depth of the resonance is determined by the line resistance. The RLC-circuits resonance frequency depends on the parasitic capacitance which makes it possible to readout the change in quantum capacitance as a small shift in the resonance frequency.

The revolutionary part of this experiment is the possibility to do readout of the charge state in a DQD without having a proximal charge sensor. All the measurement is done with the already existing leads to the dot. This opens for a much easier device design when considering coupling multiple DQDs as in [6]. Also the coupling between the qubits will be stronger because the coupling strength is not shared with an extra detector. Dispersive readout using a gate has also been demonstrated [8].

Capacitive readout in match Although the dispersive readout scheme has given beautiful results and proves a high bandwidth there is room for improvement. In multiple papers done with this measurement technique the depth of the resonance is only about 10dB or worse. This is because the readout circuit is not matched to the characteristic impedance, Z_0. The system can be matched by adding line resistance, but intuitively this is a bad thing, because more of the energy is now dissipated before even reaching the device (this agrees with simulations presented later). Matching can also be done by putting a capacitance in parallel to the parasitic capacitance. In dispersive readout this is problematic because we want to measure a change in parasitic capacitance. By adding capacitance in parallel we make the relative signal worse.

Another way to achieve a good match is to add the capacitor, C_v, in parallel to the RLC-circuit, figure 6c. This capacitor together with the inductor creates a network matching circuit that matches a resistance, which is lower than Z_0, to Z_0. In this case we want to match the line resistance, which is of the order of a few ohm, to $Z_0 = 50\Omega$. The effective impedance of the matched readout circuit is given by:

$$\frac{1}{Z_{\text{eff}}} = i\omega C_{\text{v}} + \frac{1}{i\omega L + R_l + \frac{1}{i\omega C_p}} \tag{14}$$

Because matching now is done with a capacitance, it is possible to tune into match in situ by using a varactor diode as C_{v}. The rest of this thesis will focus on characterizing dispersive readout with this circuit scheme.

4 Network matching in dispersive readout

This section focuses on describing the new network matching circuit for dispersive readout introduced above. This is done by simulations.

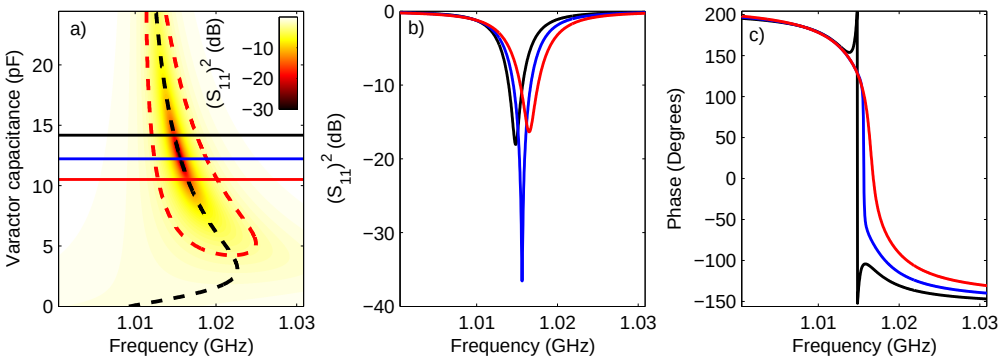

Figure 7: Simulation of power reflection coefficient from circuit in figure 6c with $L = 150\text{nH}$, $C_p = 166\text{fF}$, $R_l = 3\Omega$. a) The power reflection coefficient in dB. Black dashed line follows the resonance and red dashed line is a -3dB contour line. b) Line cuts from a) indicated with colors. c) Phase of the respective line cuts i b)

4.1 Simulations

With simulations it is possible to look into the circuits response to different changes in the circuit components. Figure 7 shows simulations with the values $L = 150\text{nH}$, $C_p = 166\text{fF}$, $R_l = 3\Omega$, and C_v as a variable. The simulations was done by substituting the effective impedance given in equation (14) into (9) with $Z_0 = 50\Omega$. (Results are shown in power reflection coefficient to be directly comparable to the measurements presented later.)

As desired it is possible to reach a match only by tuning the varactor capacitance C_v. The black dashed line maps out the resonance frequency for each value of varactor capacitance. The position and form of this line is entirely controlled by L and C_p. When the line resistance is 50Ω the RLC-circuit without the varactor capacitance is in a perfect match. For line resistances lower than 50Ω the match moves along the dashed line toward higher values of varactor capacitance. The Q-factor of the match is controlled by the line resistance. The lower the line resistance the higher the Q-factor in match. Moving away from match with the varactor capacitance will change the bandwidth shown as the red dashed line in figure 7.

We want to detect a nearly infinitesimal change in the parasitic capacitance C_p. This change will result in a small shift of the resonance frequency. As can be seen on figure 7c a 180° phase change due to a very small shift in resonance frequency is achieved in match. But this is a very deceiving result. Taking a closer look at the magnitude of the reflection coefficient 7b. There is almost no signal reflected. This is because the 180° change originates from a trivial movement across the origin in IQ-space. The phase or the amplitude of the reflected signal does not tell everything in itself.

Up till now all experiments have either focused on the change in amplitude (resistive readout) or the change in phase (dispersive readout). This has been the natural thing to do with the way the readout circuit works. In resistive reflectometry there is almost no phase change and in dispersive readout almost no amplitude change. But now wanting to simulate dispersive readout in match this is not sufficient. We have to look at both the phase and the amplitude.

4.2 Simulated response

With the tank circuit normally used in reflectometry we are actually measuring I and Q of the reflected signal. For a given set of parameter values each frequency value will

correspond to a specific point in IQ-space of the reflected signal. Changing any parameter in the circuit will move us to a different point. We want to avoid thinking about the response in the signal as either a phase shift (azimuthal change) or an amplitude change (radial change). Instead we can think of it as the distance between two points in IQ-space. The trivial 180° change originating from crossing the origin will no longer look special, because the origin is no longer special. Experimentally, one can measure along any direction in IQ space with a trivial adjustment of the phase shift.

To get the best sensitivity in dispersive readout we want to maximise this movement for changes in the parasitic capacitance C_p. To do this I have simulated the magnitude of the response as a function of frequency and total varactor capacitance C_v, assuming a change in the parasitic capacitance ΔC_p of 9aF found in [19], a carrier power of −80dBm, and a noise level of −138dBm, figure 8. The change in capacitance corresponds to an interdot transition in a DQD.

For each point I calculated the voltage reflection coefficient with the model introduced above using the same parameters: $C_p = 166\mathrm{fF}$, $R_l = 3\Omega$ and $L = 150\mathrm{nH}$. These numbers are reasonable when compared to the literature. The reflected signal defines a point in IQ-space for each value of frequency and varactor capacitance. This is shown as the middle point in figure 8b and 8c. Now making the same calculation only adding a small value $\Delta C_p = 9\mathrm{aF}$ to the parasitic capacitance I get another point in the IQ-space, second point in figure 8b and 8c. The distance between the two points is then calculated, divided by the noise level, and then plotted in figure 8a.

The SNR was determined using a noise level of −127dBm and 625μs integration time, which was calculated from the noise seen in the data. I found that the noise level is the same both in and off resonance and does not depend on the carrier power. From this I conclude that the noise originates from the cryogenic amplifier, which is the first amplifier. The noise level in the data was determined to be 14mV corresponding to −27dBm. This is the noise after amplification. Subtracting 111dB amplification gives a noise level of −138dBm.

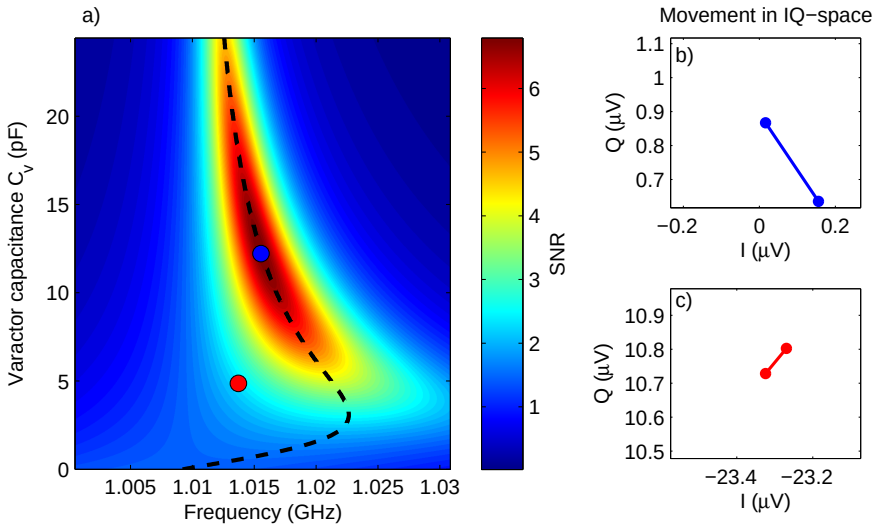

Figure 8: Simulated response with the change in C_p given by $\Delta C_p = 9\mathrm{aF}$. The response is defined as the movement in IQ-space with the −80dBm incident power and a noise level of −138dBm. a) The distance as a function of frequency and varactor bias. b-c) The distance plotted in a) at two values of varactor bias and frequency. The middle point has $\Delta C_p = 0\mathrm{aF}$ the other $\Delta C_p = 9\mathrm{aF}$.

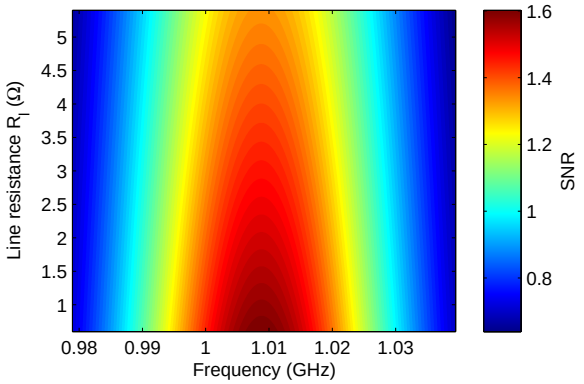

Figure 9: Same distance calculated as in figure 8 with the varactor capacitance fixed at zero.

When the varactor capacitance is zero we get a SNR of 1.4 for an interdot transition with an integration time of 625μs, which is largely consistent with 1 SNR at 350μs found in [19] for an InAs nanowire DQD. When adding varactor capacitance our SNR goes as high as 6.8. Integration time is proportional to the square of the reciprocal noise. Increasing the SNR from 1.4 to 6.8 with a varactor capacitance corresponds to 22 times faster readout. This means a readout time for interdot transitions of 16μs. The relaxation time T_1 in InAs nanowire DQDs was found to be much greater than 1μs [20], promising single-shot readout.

The amount the varactor capacitance will improve response is strongly dependent on the achievable Q-factor, which is controlled by the line resistance R_l. If $R_l = 50\Omega$ the system is already in match, and the varactor capacitance will only make the readout worse. The lower the line resistance get, the higher the Q-factor in resonance achieved by varactor tuning.

Surprisingly the best readout for the case of no varactor capacitance, just the RLC-circuit, is reached at the lowest line resistance. Meaning, as mentioned earlier, that if you try to tune the RLC-circuit into match by adding line resistance you get worse sensitivity. On figure 9 the response is in the case of no varactor capacitor.

5 Data analysis

To investigate the models validity I made measurements on the readout circuit without a device attached, and analysed the results with the model.

5.1 Setup

A picture of the circuit can be seen in figure 10. The varactors used was a MACOM MA46H070 0.3-1.2pF and a Toshiba 1SV186 0.7-4pF. In parallel to these was a 5.6pF capacitor. The bias to the varactors was supplied through a 5kΩ resistor with a 100pF capacitance to ground, such that the RF-signal sees ground. I have also added a bias-T consisting of a 220pF capacitor and a 5kΩ resistance to the voltage line, in case we wanted to connect a device. The DC-line was grounded and not used in the experiment. The inductor was a 150nH surface mount inductor. The experiments was done in a dilution refrigerator with a base temperature below 50mK to replicate actual dispersive readout as much as possible. The tank circuit used was explained in section 3.1.

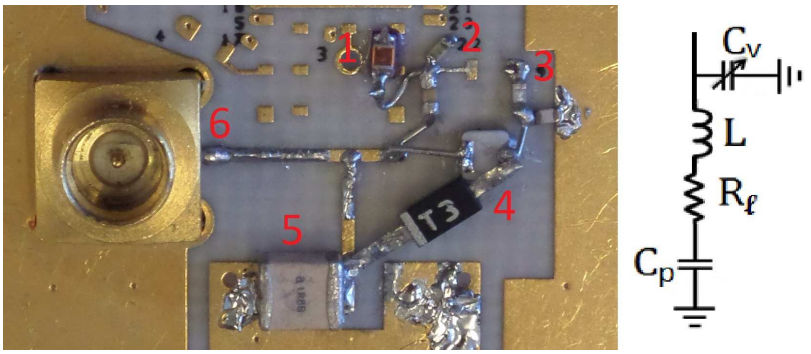

Figure 10: Picture of measured readout circuit. 1) 150nH inductor. 2) Bias-T grounded in experiment consisting of 5kΩ resistor and 220pF capacitor. 3) Varactor bias supply consisting of 5kΩ resistor and 100pF capacitor to ground. 4) The two varactors. 5) A 5.6pF capacitor to ground in parallel with the varactors. 6) RF feed line.

Figure 11a shows the magnitude of the power reflection coefficient measured with a network analyser. In the tank circuit there was more amplification coming up than attenuation going down. This explains why the power reflection coefficient measured is higher than 0dB. I found that the overall reflection increased at lower temperature. This is most likely due to some temperature dependent attenuation in the system.

The data was taken at a temperature of 45K where the match was within the range of the varactor capacitance. It was possible to tune into a match by varying the varactor bias. This proves the concept I set out to measure. However, I found that the model does not fully explain the data.

5.2 Dataset with zero varactor bias

The position of the match as a function of varactor bias changed with temperature. The temperature dependence is clear in figure 12a. Plotted is the power reflection coefficient at zero varactor bias. Calculating the varactor capacitance from datasheets gives $C_v = 13$pF at zero bias. As the temperature changes the resonance frequency moves until 33K. At lower temperatures the resonance keeps the same frequency but the depth still changes.

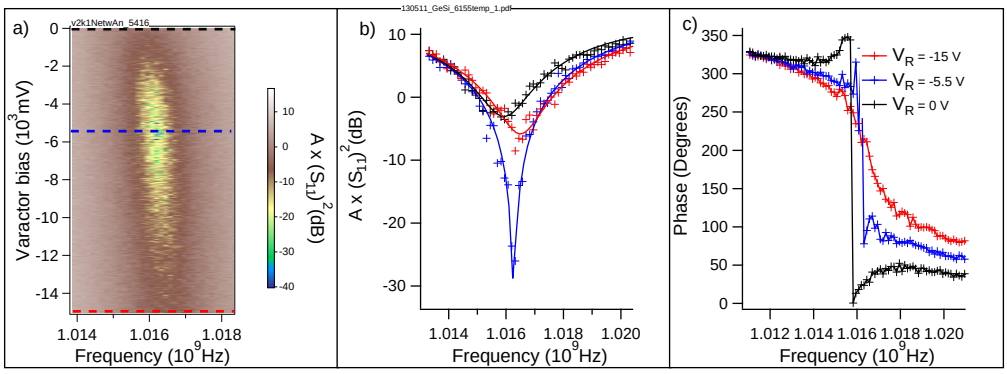

Figure 11: Data comparable to figure 7. a) Measured power reflection coefficient at 45K. b) Line cuts of the power reflection coefficient fitted with the model in figure 6c c) Phase the reflection along the lines in a.

The normalization was done to subtract the overall difference in power level at varying temperatures. The normalization factor was extracted from each dataset as a fit parameter. The fits, also normalized with the same factor, is plotted along the datasets in figure 12a. The fitting was done with the equations (9) and (14). The number which was measured by the network analyser, M, is connected to the reflection coefficient the following way:

$$M = 10\log(A) + 10\log\left(\frac{P}{P_0}\right) = 10\log\left(A\left(S_{11}\right)^2\right) = 20\log\left(\sqrt{A}S_{11}\right) \tag{15}$$

Where $10\log(A)$ is the overall gain in dB from the tank circuit. These fits allowed me to extract the circuit parameters from the datasets, figure 13(b-d). Throughout all fits in this thesis the inductance was held constant at 150nH.

We expect that the varactor capacitance extracted from the fits would have a constant value close to 13pF. What we see is around 9.5pF except for high temperatures.

For the parasitic capacitance C_p we see a linear dependence with temperature until 33K at which temperature we also see the best match. At lower temperatures C_p stays around the same value.

The form of the line resistance does not fit any of the used materials resistance temperature dependence. Had it been purely temperature dependent it would have looked almost constant. The peak is also curiously placed right when the circuit is in match.

Because this dataset has a fixed varactor capacitance I also tried to fit the data

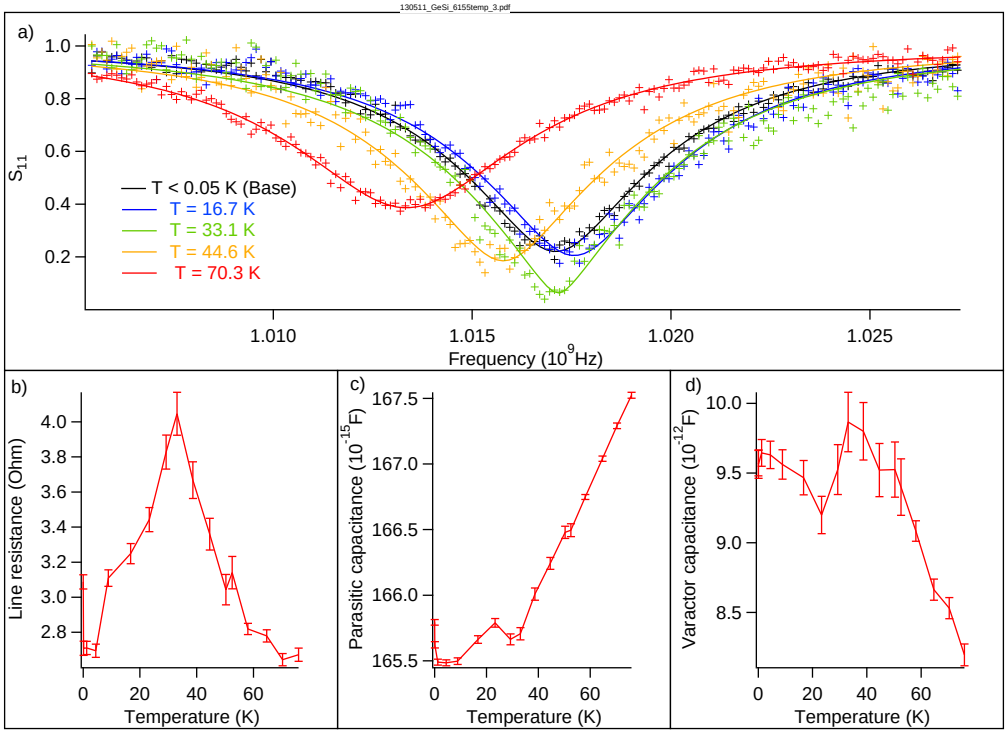

Figure 12: a) Normalized voltage reflection coefficient with 0 varactor bias at different temperatures. Fitted to the simulated model shown in figure 6c with L fixed at 150nH. Extracted values from fits for b) line resistance R_l c) parasitic capacitance C_p and varactor capacitance C_v.

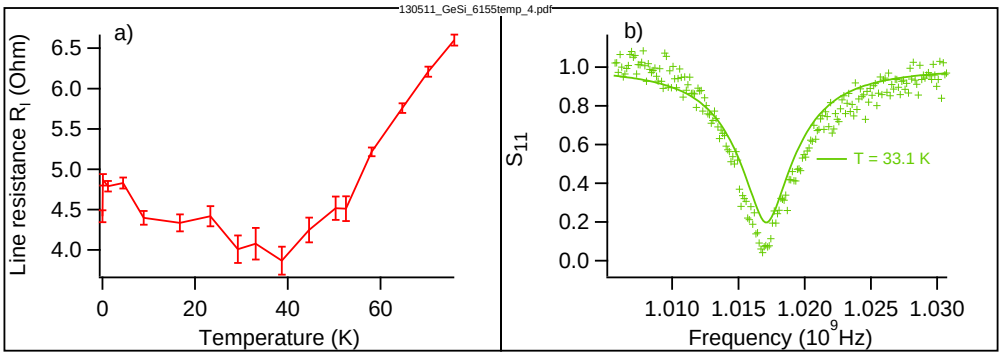

Figure 13: a) Extracted values for the line resistance R_l when $L = 150$nH and $C_v = 13$pF. b) The quality of the fits in resonance when C_v was held constant at 13pF.

keeping the varactor capacitance at the calculated 13pF in addition to the inductor at 150nH, figure 13.

The temperature dependence of the parasitic capacitance is almost unchanged from the plot in firgure 12 and is not shown. In the simulation I found that the parasitic capacitance and the inductor determined the resonance frequency, while the depth and bandwidth of the resonance was determined by the varactor capacitance and line resistance. This is also the observation we make here. Fixing the varactor capacitance at the theoretical value of 13pF only influences the line resistance. This also argues that the temperature at which the parasitic capacitance stabilizes is uncorrelated to the match.

For the line resistance we see that the peak disappears, but now we see a temperature dependence at higher temperature. Furthermore this is definitely not an optimal fit as can be seen in firgure 13b. Leading us to conclude that the assumption of $C_\mathrm{v} = 13$pF is likely not true.

Fixing $C_\mathrm{v} = 9.5$pF gives good fits, which is achieved by lowering the line resistance by aboout $0.1-0.3\Omega$ at high temperatures where the varactor capacitance was substantially different from 9.5pF. Fixing the value of the line resistance at 3Ω instead also gives good fits at the cost of a small peak in the varactor capacitance around the resonance.

Above we are plotting a resonance with 3 or 4 parameters. With this amount of parameters it is not surprising that we can get good fits even if the model is not entirely true. The model compensates for that by letting the parameters vary in a non-physical way. Which I think is the explanation for the peak in line resistance around match.

5.3 Data at constant temperature

The data in figure 9 was taken at a constant temperature. Fitting these resonance lines will allow us to see how the fit parameters behave when crossing the match by varying the varactor capacitance.

I fixed the value of the parasitic capacitance to $C_p = 166.25$fF under the assumption, that the observed change in figure 12 is due to temperature change only. On figure 14 the movement of the varactor capacitance and the line resistance are shown.

Even with both C_p and L fixed the fits looked good both in match and out of match, which supports the hypothesis that the change in parasitic capacitance is only temperature dependent.

The movement of the varactor capacitance as a function of varactor bias is in the correct diretion, but it is too small compared to the datasheets. In both this dataset and the set above we see the varactor behaving different from the datasheets. This could be

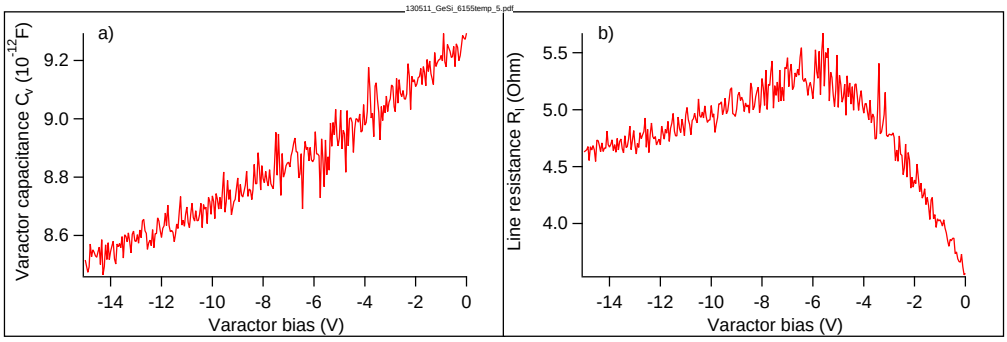

Figure 14: Extracted values from fitting the resonance lines in figure 12a. with $L = 150$nH and $C_p = 166.25$fF.

a physical change due to temperature. We again see a peak in the line resistance around the resonance. From this together with the observations in the subsection above we can conclude that it is most likely an incorrect model we are using.

A plausible correction to the model may be found in the inductor. The inductor manufacturer has a model, which includes a capacitor and resistor in parallel to the inductor. I did not have time to make any fits with this model. However, I made a few calculation to consider the impact on my simulations. The premature results show that the overall picture presented in section 4.1 and 4.2 is unchanged. From this I conclude that my simulation still holds, although it is with added uncertainty to the quantitative numbers.

6 Conclusion

A simple varactor diode was introduced into the dispersive readout scheme. Simulations show that the varactor diode allows for in situ tuning of the match in the resonant readout circuit. I found that characterizing the dispersive readout response as either a phase or amplitude change is insufficient. Instead I propose characterization of signal as the magnitude of change in IQ-space. This allowed me to do measurement simulations with a dispersive shift of 9aF.

These results indicates 22 times faster readout times compared to the current dispersive readout circuit. The increase in sensitivity should enable single shot readout in InAs singlet-triplet qubits, and will also be useful as a general improvement for dispersive readout. Viable readout methods for qubits without a separate mesoscopic structure would greatly simplify scaled up systems.

Experiments were performed on the new readout circuit to prove or disprove the validity of the simulated model. It was possible to tune the resonance of the circuit as desired. However, changes in fitting parameters do not quantitatively agree with the physical expectations of the different electrical components. This hints that the simulated model does not completely explain the circuit. The fact that it was possible to tune into a match using only the varactor diode and the general qualitative agreement with the model argue that the simulation might only need a small correction.

In further studies it could be interesting to fit the data using the more elaborate model for the surface mount inductor. The next experimental step will be to attach a device and experimentally demonstrate sensitivity sufficient for single-shot readout.

7 References

[1] D. P. DiVincenzo, *Quantum Computation*, Science **270**, 255 (1995).

[2] D. P. DiVincenzo, *The Physical Implementation of Quantum Computation*, Fortschr. Phys. **48**, 771 (2000).

[3] D. Loss and D. P. DiVincenzo, *Quantum computation with quantum dots*, Physical Review A **57**, 120 (1998).

[4] J. R. Petta, A. C. Johnson, J. M. Taylor, E. A. Laird, A. Yacoby, M. D. Lukin, C. M. Marcus, M. P. Hanson, and A. C. Gossard, *Coherent Manipulation of Coupled Electron Spins in Semiconductor Quantum Dots*, Science **309**, 2180 (2005).

[5] H. Bluhm, S. Foletti, I. Neder, M. Rudner, D. Mahalu, V. Umansky, and A. Yacoby, *Dephasing time of GaAs electron-spin qubits coupled to a nuclear bath exceeding 200μs*, Nature Physics **7**, 109 (2011).

[6] M. D. Shulman, O. E. Dial, S. P. Harvey, H. Bluhm, V. Umansky, and A. Yacoby, *Demonstration of Entanglement of Electrostatically Coupled Singlet-Triplet Qubits*, Science **336**, 202 (2012).

[7] C. Barthel, D. J. Reilly, C. M. Marcus, M. P. Hanson, and A. C. Gossard, *Rapid Single-Shot Measurement of a Singlet-Triplet Qubit*, Physical Review Letters **103**, 160503 (2009).

[8] J. I. Colless, A. C. Mahoney, J. M. Hornibrook, A. C. Doherty, H. Lu, A. C. Gossard, and D. J. Reilly, *Dispersive Readout of a Few-Electron Double Quantum Dot with Fast rf Gate Sensors*, Physical Review Letters **110**, 046805 (2013).

[9] W. G. van der Wiel, S. De Franceschi, J. M. Elzerman, T. Fujisawa, S. Tarucha, and L. P. Kouwenhoven, *Electron transport through double quantum dots*, Reviews of Modern Physics **75** (2003).

[10] T. A. Fulton and G. J. Doaln, *Observation of single-electron charging effects in small tunnel junctions*, Physical Review Letters **59**, 109 (1987).

[11] R. Hanson, L. P. Kouwenhoven, J. R. Petta, S. Tarucha, and L. M. K. Vandersypen *Spins in few-electron quantum dots*, Reviews of Modern Physics **79** (2007).

[12] M. Field, C. G. Smith, M. Pepper, D. A. Ritchie, J. E. F. Frost, G. A. C. Jones, and D. G. Hasko, *Measurements of Coulomb blockade with a noninvasive voltage probe*, Physical Review Letters **70**, 1311 (1993).

[13] K. D. Petersson, C. G. Smith, D. Anderson, P. Atkinson, G. A. C. Jones, and D. A. Ritchie, *Charge and spin state readout of a double quantum dot coupled to a resonator*, Nano Letters **8**, 2789 (2010).

[14] R. J. Schoelkopf, P. Wahlgren, and A. Kozhevnikov, P. Delsing, and D. E. Prober, *The radio-frequency single-electron transistor (RF-SET): a fast and ultrasensitive electrometer*, Science **280**, 1238 (1998).

[15] D. J. Reilly, C. M. Marcus, M. P. Hanson, and A. C. Gossard, *Fast single-charge sensing with a rf quantum point contact*, Applied Physics Letters **91**, 162101 (2007).

[16] M. C. Cassidy, A. S. Dzurak, R. G. Clark, K. D. Petersson, I. Farrer, D. A. Ritchie, and C. G. Smith, *Single shot charge detection using a radio-frequency quantum point contact*, Applied Physics Letters **91**, 222104 (2007).

[17] J. Bylander, T. Duty, and P. Delsing, *Current measurement by real-time counting of single electrons*, Nature **434**, 361 (2005).

[18] C. Barthel, M. Kjærgaard, J. Medford, C. M. Marcus, P. Hanson, and A. C. Gossard, *Fast sensing of double-dot charge arrangement and spin state with a radio-frequency sensor quantum dot*, Physical Review B **81**, 161308 (2010).

[19] M. Jung, M. Schroer, and K. D. Petersson, and J. R. Petta, *Radio frequency charge sensing in InAs nanowire double quantum dots*, Applied Physics Letters **100**, 253508 (2012).

[20] S. Nadj-Perge, S. M. Frolov, E. P. A. M. Bakkers, and L. P. Kouwenhoven, *Spin–orbit qubit in a semiconductor nanowire*, Nature **468**, 1084 (2010).